Inorg. Chem. **2003**, *42*, 2031–2039

Semiconducting Perovskites $(2\text{-}XC_6H_4C_2H_4NH_3)_2SnI_4$ (X = F, Cl, Br): Steric Interaction between the Organic and Inorganic Layers

Zhengtao Xu, David B. Mitzi,* Christos D. Dimitrakopoulos, and Karen R. Maxcy

IBM T. J. Watson Research Center, P.O. Box 218, Yorktown Heights, New York 10598

Received October 30, 2002

Two new semiconducting hybrid perovskites based on 2-substituted phenethylammonium cations, $(2\text{-}XC_6H_4C_2H_4NH_3)_2SnI_4$ (X = Br, Cl), are characterized and compared with the previously reported X = F compound, with a focus on the steric interaction between the organic and inorganic components. The crystal structure of $(2\text{-}ClC_6H_4C_2H_4NH_3)_2SnI_4$ is solved in a disordered subcell [*C*2/*m*, $a = 33.781(7)$ Å, $b = 6.178(1)$ Å, $c = 6.190(1)$ Å, $\beta = 90.42(3)°$, and $Z = 2$]. The structure is similar to the known $(2\text{-}FC_6H_4C_2H_4NH_3)_2SnI_4$ structure with regard to both the conformation of the organic cations and the bonding features of the inorganic sheet. The $(2\text{-}BrC_6H_4C_2H_4NH_3)_2SnI_4$ system adopts a fully ordered monoclinic cell [$P2_1/c$, $a = 18.540(2)$ Å, $b = 8.3443(7)$ Å, $c = 8.7795(7)$ Å, $\beta = 93.039(1)°$, and $Z = 2$]. The organic cation adopts the anti conformation, instead of the gauche conformation observed in the X = F and Cl compounds, apparently because of the need to accommodate the additional volume of the bromo group. The steric effect of the bromo group also impacts the perovskite sheet, causing notable distortions, such as a compressed Sn–I–Sn bond angle (148.7°, as compared with the average values of 153.3 and 154.8° for the fluoro and chloro compounds, respectively). The optical absorption features a substantial blue shift (lowest exciton peak: 557 nm, 2.23 eV) relative to the spectra of the fluoro and chloro compounds (588 and 586 nm, respectively). Also presented are transport properties for thin-film field-effect transistors (TFTs) based on spin-coated films of the two hybrid semiconductors.

Introduction

Organic−inorganic perovskites have recently attracted considerable attention, mainly because such compounds may combine useful properties from the inorganic as well as the organic moieties within a crystalline molecular scale composite.[1] In these systems, the inorganic portion consists of metal halide octahedral units (e.g. SnX_6^{2-}, PbX_6^{2-}, CdX_6^{2-}, etc) connected into perovskite-like layers through corner-sharing. The organic portion is usually an organic ammonium cation, balancing the negative charge from the inorganic layer. The inorganic moiety offers potential advantages such as good electrical mobility,[2−5] band gap tunability,[3−8] mechanical and thermal stability, and interesting magnetic[9] or dielectric transitions.[10] Meanwhile, the organic moiety offers useful properties such as plastic mechanical properties, convenient processing, as well as structural and functional diversity. In view of the synthetic flexibility of organic materials, this latter set of possibilities is particularly moving for the imagination.

The well-known compound $(C_6H_5CH_2CH_2NH_3)_2SnI_4$ $[(PEA)_2SnI_4]$[2,11] illustrates the above points. The tin(II) iodide

* To whom correspondence should be addressed. E-mail: dmitzi@us.ibm.com.

(1) For a recent review, see: Mitzi, D. B. *Prog. Inorg. Chem.* **1999**, *48*, 1.
(2) (a) Kagan, C. R.; Mitzi, D. B.; Dimitrakopoulos, C. D. *Science* **1999**, *286*, 945. (b) Mitzi, D. B.; Chondroudis, K.; Kagan, C. R. *IBM J. Res. Dev.* **2001**, *45*, 29.
(3) Mitzi, D. B.; Feild, C. A.; Harrison, W. T. A.; Guloy, A. M. *Nature* **1994**, *369*, 467.
(4) Mitzi, D. B.; Wang, S.; Feild, C. A.; Chess, C. A.; Guloy, A. M. *Science* **1995**, *267*, 1473.
(5) Mitzi, D. B.; Feild, C. A.; Schlesinger, Z.; Laibowitz, R. B. *J. Solid State Chem.* **1995**, *114*, 159.
(6) Mitzi, D. B. *Chem. Mater.* **1996**, *8*, 791.
(7) Papavassiliou, G. C.; Koutselas, I. B. *Synth. Met.* **1995**, *71*, 1713.
(8) (a) Weber, D. *Z. Naturforsch.* **1979**, *34b*, 939. (b) Weber, D. *Z. Naturforsch.* **1978**, *33b*, 862.
(9) (a) De Jongh, L. J.; Botterman, A. C.; De Boer, F. R.; Miedema, A. R. *J. Appl. Phys.* **1969**, *40*, 1363. (b) De Jongh, L. J.; Miedema, A. R. *Adv. Phys.* **1974**, *23*, 1. (c) Willett, R.; Place, H.; Middleton, M. *J. Am. Chem. Soc.* **1988**, *110*, 8639. (d) Long, G. S.; Wei, M.; Willett, R. D. *Inorg. Chem.* **1997**, *36*, 3102. (e) Sekine, T.; Okuno, T.; Awaga, K. *Inorg. Chem.* **1998**, *37*, 2129.
(10) (a) Levstik, A.; Filipič, C.; Blinc, R.; Arend, H.; Kind, R. *Solid State Commun.* **1976**, *20*, 127. (b) Kind, R.; Plesko, S.; Günter, P.; Roos, J.; Fousek, J. *Phys. Rev. B: Condens. Matter* **1981**, *23*, 5301. (c) Onoda-Yamamuro, N.; Matsuo, T.; Suga, H. *J. Phys. Chem. Solids* **1992**, *53*, 935.
(11) Papavassiliou, G. C.; Koutselas, I. B.; Terzis, A.; Whangbo, M.-H. *Solid State Commun.* **1994**, *91*, 695.

10.1021/ic0261474 CCC: $25.00
Published on Web 02/25/2003

sheet provides a semiconducting medium with a band gap of around 2.2 eV, and the strong covalent/ionic Sn−I bonds result in a relatively high charge carrier mobility. The organic cation meanwhile enables the compound to self-assemble to form high-quality thin films with a preferred crystallographic orientation. As a result, organic−inorganic thin-film transistors (TFTs) have been made with $(PEA)_2SnI_4$ as the channel layer.[2] Such hybrid TFT devices yield saturation-regime mobilities (~0.6 $cm^2\ V^{-1}\ s^{-1}$) comparable to that of amorphous silicon (a-Si), and such materials can in general be deposited from common organic solvents at ambient temperatures. Recent research[12] further demonstrates that $(PEA)_2SnI_4$-based TFT devices can be fabricated through melt processing, thus providing another versatile and solvent-free method of depositing semiconductive materials. Melt processing yields larger grain sizes in the channel layer and significantly improved charge carrier mobilities in both the saturation and linear regime (up to 2.6 and 1.7 $cm^2\ V^{-1}\ s^{-1}$, respectively).

Modifications on the organic cation site may influence the bonding features of the tin(II) iodide framework and the resultant electronic properties. For instance, a recent paper[13] deals with a series of (fluorophenethyl)ammonium-based perovskites. Therein, a fluoro group is substituted on the 2, 3, or 4 positions of the phenyl group in the prototypical compound $(PEA)_2SnI_4$. In so doing the authors decrease the Sn−I−Sn bond angle between the adjacent SnI_6 octahedra progressively as the fluorine atom is shifted from the 4 to the 3 and then to the 2 position. Such structural changes were found to correlate with the progressive increase of the energy of the exciton state as well as with the shift of the band edge. The structural modifications hence expand the range of potentially useful semiconductive materials. It is, however, difficult in this case to pinpoint the factors accountable for the changes in the crystal structures, as shifting the F atom on the phenyl ring could simultaneously affect various intermolecular forces governing the crystal structure.

In this paper, we focus on using steric interaction to influence the structures of the tin(II) iodide framework as well as the organic layer. As 2-position substituents on the phenyl group are located closest to the inorganic framework, these substituents are expected to most strongly affect the steric interaction between the organic molecules and the inorganic framework. As compared with the previously reported X = F system,[13] here we have chosen the bulkier Cl and Br atoms as new substituents to probe the steric impact. The corresponding compounds are formulated as $(2\text{-}ClC_6H_4CH_2CH_2NH_3)_2SnI_4$ [$(2\text{-}ClPEA)_2SnI_4$] and $(2\text{-}BrC_6H_4CH_2CH_2NH_3)_2SnI_4$ [$(2\text{-}BrPEA)_2SnI_4$]. As the chloro and bromo groups progressively pose a larger volume at the interface between the organic and inorganic components, two aspects of the consequential structural changes are interesting to consider. First, the organic molecules may adopt different conformation as well as different packing motifs in the crystal lattice. Second, the inorganic framework can distort in certain ways to accommodate the added volume.

First presented will be the crystallographic study of $(2\text{-}ClPEA)_2SnI_4$ and $(2\text{-}BrPEA)_2SnI_4$. Both compounds continue to crystallize in the generic layered perovskite structure. While the crystal structure of $(2\text{-}ClPEA)_2SnI_4$ remains similar to that of $(2\text{-}FPEA)_2SnI_4$, $(2\text{-}BrPEA)_2SnI_4$ develops distinct structural features in both the inorganic framework and the organic molecules. We will discuss major features of the crystal structures in light of the shape, volume, and packing of the molecules, so as to delineate the steric effect of the halogen substituents on the solid-state structure. Also presented are the optical absorption spectra, the film morphologies, and transport properties of the thin-film field-effect transistors based on these compounds.

Experimental Section

Crystallization of $(2\text{-}BrPEA)_2SnI_4$. $(2\text{-}BrPEA)_2SnI_4$ crystals were grown by slowly evaporating a methanol/toluene solution containing the organic and inorganic salts. First, 45.5 mg (0.122 mmol) of SnI_2 (Aldrich, anhydrous beads, 99.999%) and 80.0 mg (0.244 mmol) of (2-bromophenethyl)ammonium iodide were added to a vial under an inert atmosphere. This mixture was then dissolved in 1.0 mL of anhydrous methanol to form a yellow solution, which was then filtered through a Teflon filter (pore size: 0.2 μm). The filtrate was mixed with 2.0 mL of anhydrous toluene and placed in a loosely capped vial. Slow evaporation over a period of 3 days led to the formation of platelike, bright red crystals (120 mg, yield 95%) suitable for X-ray single-crystal analysis. The powder X-ray diffraction pattern of the product showed a single phase, consistent with the single-crystal structure. Chemical analysis of the product $(C_{16}H_{22}Br_2N_2)SnI_4$ yielded the following. Calcd: C, 18.69; H, 2.16; N, 2.72. Found: C, 18.72; H, 2.24; N, 2.74. For deposition of thin films for optical and electrical property studies, the product was first recrystallized through evaporation of a methanol/toluene solution (as described above).

Crystallization of $(2\text{-}ClPEA)_2SnI_4$. $(2\text{-}ClPEA)_2SnI_4$ crystals were grown in a process similar to that for $(2\text{-}BrPEA)_2SnI_4$. The following is the amount of reagents used in a typical run: 52.3 mg (0.140 mmol) of SnI_2; 80.0 mg (0.282 mmol) of (2-chlorophenethyl)ammonium iodide; 1.5 mL of methanol; 3.0 mL of toluene. The resultant crystals (126 mg, yield 95%) were thinner and exhibited a darker red color than the bromo analogue. The powder X-ray diffraction pattern of the product showed a single phase consistent with the single-crystal structure. Chemical analysis of the product $(C_{16}H_{22}Cl_2N_2)SnI_4$ yielded the following. Calcd: C, 20.45; H, 2.36; N, 2.98. Found: C, 20.34; H, 2.24; N, 2.94. For deposition of thin films for optical and electrical property studies, the product was first recrystallized through evaporation of a methanol/toluene solution (as described above).

X-ray Crystallography. A blocklike crystal of $(2\text{-}BrPEA)_2SnI_4$ was selected under a microscope and attached to the end of a quartz fiber with 5 min epoxy. A full sphere of data was collected at room temperature on a Bruker SMART CCD diffractometer, equipped with a normal focus 2.4 kW sealed tube X-ray source (Mo Kα radiation). Intensity data were collected with a detector distance of approximately 5.0 cm, in 2272 frames with increasing ω. The increment in ω between each frame was 0.3°. An empirical absorption correction based on equivalent reflections was applied to the intensity data.[14] The structure was solved and refined with Shelxl 97. First, the Sn, I, and Br atoms were located by direct

(12) Mitzi, D. B.; Dimitrakopoulos, C. D.; Rosner, J.; Medeiros, D. R.; Xu, Z.; Noyan, C. *Adv. Mater.* **2002**, *14*, 1772.
(13) Mitzi, D. B.; Dimitrakopoulos, C. D.; Kosbar, L. L. *Chem. Mater.* **2001**, *13*, 3728.

Table 1. Crystallographic Data for (2-BrPEA)$_2$SnI$_4$ and (2-ClPEA)$_2$SnI$_4$

	(2-BrPEA)$_2$SnI$_4$	(2-ClPEA)$_2$SnI$_4$
chem formula	$C_{16}H_{22}N_2Br_2SnI_4$	$C_{16}H_{22}N_2Cl_2SnI_4$
fw	1028.50	939.59
space group	$P2_1/c$ (No. 14)	$C2/m$ (No. 12)
a, Å	18.540(2)	33.781(7)
b, Å	8.3443(7)	6.178(1)
c, Å	8.7795(7)	6.190(1)
β, deg	93.039(1)	90.42(3)
V, Å^3	1356.3(2)	1291.8(4)
Z	2	2
ρ_{calcd}, g/cm^3	2.518	2.415
wavelength, Å	0.710 73 (Mo Kα)	0.710 73 (Mo Kα)
abs coeff (μ), cm^{-1}	84.45	59.80
R$_1$[a]	0.0370 ($I > 2\sigma(I)$)	0.0468 ($I > 2\sigma(I)$)
wR$_2$[b]	0.1060 ($I > 2\sigma(I)$)	0.1354 ($I > 2\sigma(I)$)

[a] $R_1 = \sum(|F_o| - |F_c|)/\sum(|F_o|)$. [b] $wR2 = \{\sum[w(F_o^2 - F_c^2)^2]/\sum[w(F_o^2)^2]\}^{1/2}$.

methods. The N and C atoms were then located using successive Fourier difference maps. Hydrogen atoms were either located by Fourier difference map or added at idealized positions. All non-hydrogen atoms (Sn, I, C, N, and Br) were refined anisotropically. The minimum and maximum peaks in the final difference Fourier maps corresponded to −1.262 and 1.359 e/Å^3.

The crystallographic dataset for (2-ClPEA)$_2$SnI$_4$ was collected and processed in a similar manner. However, two aspects of the structure solution and refinement are noteworthy. First, this crystal structure was solved from a twinned crystal in the space group $C2/m$ [a = 33.781(7) Å, b = 6.178(1) Å, c = 6.190(1) Å, β = 90.42(3)°, and $Z = 2$]. The twinning is pseudomerohedral, and the twin law R = (100, 0$\bar{1}$0, 00$\bar{1}$) was applied in the structure refinement using the SHELXL program. The twinning was first suspected from the value of the β angle, which gives a higher metric symmetry (orthorhombic) than the Laue symmetry (monoclinic). The twinning was further confirmed by the following features:[15] (1) Some reflection peaks are split into doublets. (2) K = mean-(F_o^2)/mean(F_c^2) is systematically very high for reflections with low intensity, and there are quite a few high residual peaks with densities of more than 1 e/Å^3 after the last cycle of refinement without the twinning command. (3) Inclusion of the twin law in the refinement substantially lowers the R1 value (e.g., from 6.5% to 4.7%) as well as the electron densities of the residual peaks (the minimum and maximum peaks in the final difference Fourier maps corresponded to −0.670 and 0.968 e/Å^3). Aside from the twinning phenomenon, the X-ray diffractions produce on the CCD frames sharp, well-defined spots as well as some streaks (indicating some disorder or unresolved superstructure), as has been seen in many other tin(II) iodide-based hybrid structures.[13] The current subcell was first indexed from the sharp reflections handpicked from the CCD frames and then refined in the integration process.

Selected crystallographic results for both compounds are summarized in Table 1. The atomic coordinates are listed in Tables 2 and 3. Selected bond distances and angles are summarized in Tables 4 and 5. A complete listing of crystallographic data, along with anisotropic displacement parameters for each compound, is given as Supporting Information.

Thin Film Deposition. Films of the (2-ClPEA)$_2$SnI$_4$ and (2-BrPEA)$_2$SnI$_4$ perovskites were prepared in a nitrogen-filled drybox by spin-coating a methanol solution of the perovskites (20 mg perovskite/1.6 mL methanol) on quartz substrates. The substrate surface was first flooded by the solution, and a spinning cycle was then initiated (1 s ramp to 3000 rpm; dwell 30 s at 3000 rpm). The substrate was then annealed at 70 °C for 15 min to remove residual solvent and improve film quality. The films thus formed exhibited well-defined (h00) X-ray diffraction peaks, indicating that the films were well crystallized and highly oriented. The film morphology was also studied by atomic force microscopy (AFM) in the tapping mode (NanoScope IIIa, Dimension 3100, Digital Instruments, Santa Barbara CA), with the scan area being 2 × 2 μm for each sample. All the experimental details are the same as previously reported.[13]

Table 2. Atomic Coordinates and Equivalent Isotropic Displacement Coefficients (Å^2 × 10^2)[a] for (2-BrPEA)$_2$SnI$_4$

atom	x	y	z	U(eq)
Sn	0.0	0.5	0.0	4.0(1)
I(1)	0.0292(1)	0.3064(1)	0.3049(1)	5.7(1)
I(2)	0.1671(1)	0.5720(1)	0.0011(1)	6.5(1)
N	0.1474(4)	0.5138(9)	0.594(1)	7.6(2)
C(1)	0.234(1)	0.454(2)	0.587(1)	14.1(5)
C(2)	0.238(1)	0.423(2)	0.441(2)	18.5(8)
C(3)	0.3251(5)	0.376(1)	0.447(2)	12.3(4)
C(4)	0.3763(4)	0.471(1)	0.388(1)	8.7(2)
C(5)	0.4450(7)	0.416(2)	0.363(2)	12.8(4)
C(6)	0.4589(8)	0.255(2)	0.383(2)	14.9(5)
C(7)	0.4073(9)	0.156(2)	0.438(2)	14.0(5)
C(8)	0.3434(7)	0.2124(2)	0.469(2)	14.6(6)
Br	0.3562(1)	0.6920(2)	0.3518(2)	14.2(1)

[a] Equivalent isotropic U defined as one-third of the trace of the orthogonalized U_{ij} tensor. Positions and isotropic thermal parameters for the hydrogen atoms and anisotropic thermal parameters for the other atoms are listed in the Supporting Information.

Table 3. Atomic Coordinates and Equivalent Isotropic Displacement Coefficients (Å^2 × 10^2)[a] for (2-ClPEA)$_2$SnI$_4$

atom	x	y	z	U(eq)
Sn	0.0	0.0	0.5	4.2(1)
I(1)	0.0934(1)	0.0	0.4890(3)	6.1(1)
I(2)	−0.0001(1)	0.5	0.3894(3)	5.3(1)
I(3)	0.0	−0.1134(3)	0.0	5.0(1)
N(1a)	0.0815(7)	0.5	0.172(4)	5.1(5)
N(1b)	0.0797(9)	0.343(9)	0.004(8)	10(2)
C(1)	0.0976(5)	0.5	0.000(7)	10.5(8)
C(2)	0.1408(6)	0.594(4)	−0.038(5)	8.0(8)
C(3)	0.1685(6)	0.392(3)	0.032(4)	5.4(5)
C(4)	0.1889(7)	0.392(4)	0.222(4)	6.3(6)
C(5)	0.2168(8)	0.225(5)	0.282(5)	8.0(8)
C(6)	0.2237(9)	0.065(6)	0.149(7)	10(1)
C(7)	0.2019(9)	0.060(4)	−0.076(6)	10(1)
C(8)	0.1745(8)	0.239(5)	−0.113(4)	7.8(7)
Cl	0.1830(3)	0.408(2)	0.410(1)	10.3(3)

[a] Equivalent isotropic U defined as one-third of the trace of the orthogonalized U_{ij} tensor. Positions and isotropic thermal parameters for the hydrogen atoms and anisotropic thermal parameters for the other atoms are listed in the Supporting Information.

Table 4. Selected Bond Distances (Å) and Angles (deg) for (2-ClPEA)$_2$SnI$_4$

Sn−I(1)	3.156(1)	I(2)[a]−Sn−I(2)	180
Sn−I(1)[a]	3.156(1)	I(1)[a]−Sn−I(3)[a]	88.38(4)
Sn−I(2)	3.1639(7)	I(1)−Sn−I(3)[a]	91.62(4)
Sn−I(2)[a]	3.1639(7)	I(2)[a]−Sn−I(3)[a]	90.26(4)
Sn−I(3)	3.1734(7)	I(2)−Sn−I(3)[a]	89.74(4)
Sn−I(3)[a]	3.1734(7)	I(1)[a]−Sn−I(3)	91.62(4)
		I(1)−Sn−I(3)	88.38(4)
I(1)[a]−Sn−I(1)	180	I(2)[a]−Sn−I(3)	89.74(4)
I(1)[a]−Sn−I(2)[b]	89.71(5)	I(2)−Sn−I(3)	90.26(4)
I(1)−Sn−I(2)[b]	90.29(5)	I(3)[a]−Sn−I(3)	180
I(1)[a]−Sn−I(2)[a]	89.71(5)	Sn[c]−I(2)−Sn	155.02(6)
I(1)−Sn−I(2)[a]	90.29(5)	Sn−I(3)−Sn[d]	154.50(6)

[a] $-x, -y, -z + 1$. [b] $-x, -y + 1, -z + 1$. [c] $x, y + 1, z$. [d] $x, y, z - 1$.

(14) Sheldrick, G. M. *SADABS*; Institut für Anorganische Chemie der Universität Göttingen: Göttingen, Germany, 1997.
(15) Herbst-Irmer, R.; Sheldrick, G. M. *Acta Crystallogr., Sect. B* **1998**, *54*, 443.

Table 5. Selected Bond Distances (Å) and Angles (deg) for $(2\text{-BrPEA})_2SnI_4$

$Sn^a-I(1)$	3.1407(4)	$I(1)-Sn-I(1)^d$	180
$Sn-I(1)$	3.1484(4)	$I(1)^b-Sn-I(2)^d$	87.66(1)
$Sn-I(1)^c$	3.1407(4)	$I(1)^c-Sn-I(2)^d$	92.34(1)
$Sn-I(1)^d$	3.1484(4)	$I(1)-Sn-I(2)^d$	91.68(1)
$Sn-I(2)^d$	3.1551(4)	$I(1)^d-Sn-I(2)^d$	88.32(1)
$Sn-I(2)$	3.1551(4)	$I(1)^b-Sn-I(2)$	92.34(1)
$I(1)^b-Sn-I(1)^c$	180	$I(1)^c-Sn-I(2)$	87.66(1)
$I(1)^b-Sn-I(1)$	88.897(7)	$I(1)-Sn-I(2)$	88.32(1)
$I(1)^c-Sn-I(1)$	91.103(7)	$I(1)^d-Sn-I(2)$	91.68(1)
$I(1)^b-Sn-I(1)^d$	91.103(7)	$I(2)^d-Sn-I(2)$	180
$I(1)^c-Sn-I(1)^d$	88.897(7)	$Sn^a-I(1)-Sn$	148.71(1)

^{a} $-x, y-0.5, -z+0.5$. ^{b} $-x, y+0.5, -z+0.5$. ^{c} $x, -y+0.5, z-0.5$. ^{d} $-x, -y+1, -z$.

Optical Properties. Absorption spectra were obtained at room temperature on spin-coated films (deposited on quartz disks) of both the $(2\text{-ClPEA})_2SnI_4$ and $(2\text{-BrPEA})_2SnI_4$ compounds. The instrument is a Hewlett-Packard UV−vis 8543 spectrophotometer.

Electrical Measurements. Thin-film field-effect transistors (TFT) based on both the $(2\text{-ClPEA})_2SnI_4$ and $(2\text{-BrPEA})_2SnI_4$ compounds were tested using a Hewlett-Packard 4145B semiconductor analyzer. The organic−inorganic TFT consists of a heavily n-doped silicon wafer as the gate, 5000 Å thick thermally grown oxide gate dielectric, Pd source and drain electrodes with a chromium adhesion layer (deposited by evaporation through a silicon membrane shadow mask[16]), and the spin-coated organic−inorganic hybrid channel material. The source and drain electrodes are deposited directly on the gate dielectric, followed by deposition of the hybrid material. Channel length (L), defined as the distance between the source and drain electrode, ranged from 5 to 95 μm, while channel width (W) ranged from 250 to 1500 μm. Devices were fabricated, maintained, and tested in a nitrogen-filled drybox with oxygen and water levels below 1 ppm.

Results and Discussion

Crystal Structures. Despite the more bulky substituents at the 2-position of the phenyl ring relative to the X = F system, both $(2\text{-ClPEA})_2SnI_4$ and $(2\text{-BrPEA})_2SnI_4$ continue to adopt a layered structure, comprised of tin(II) iodide perovskite sheets alternating with organic cation layers (Figures 1 and 2). Note that the formation of the perovskite sheet is highly dependent on electrostatic and hydrogen-bonding interaction between the ammonium group and the tin(II) iodide component.[17] As can be seen in Figures 1 and 2, the ammonium groups extend into the tin(II) iodide layer. Too much steric hindrance around the ammonium group would therefore disrupt the formation of the perovskite sheet. Another factor that could influence the formation of the perovskite structure is the cross-sectional area of the organic cation.[17] If this area is larger than that of the square-like area provided by the four adjacent SnI_6 octahedra (e.g., see Figure 3), nearest-neighbor organic cations would interfere and the perovskite structure would not form. If, on the other hand, the cross-sectional area is substantially smaller, the organic cations can adopt a tilted orientation relative to the inorganic sheet and thereby achieve a stable packing motif. Here the chloro and bromo groups, placed at the 2-position of the phenyl group, prove compatible with the perovskite structure, indicating that both the steric hindrance around the ammonium group and the cross-sectional area of the organic cation are within the tolerance of this type of structure. Of interest, however, is how the chloro and bromo groups modify the overall crystal structures and, in particular, the structural details of the perovskite sheet.

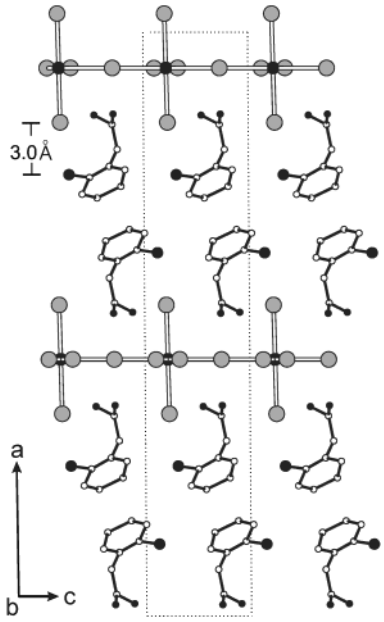

Figure 1. Crystal structure of $(2\text{-ClPEA})_2SnI_4$ viewed along the b axis. Open bonds are used for the tin(II) iodide sheet, and filled bonds for the organic cations. Sn: large black sphere. I: gray sphere. C: small open sphere. N: small black sphere. Cl: medium black sphere. The number (3.0 Å) refers to the distance between the plane of the chlorine atoms and that of the apical iodine atoms.

The crystal structure of $(2\text{-ClPEA})_2SnI_4$ was solved in a disordered monoclinic subcell [$C2/m$, $a = 33.781(7)$ Å, $b = 6.178(1)$ Å, $c = 6.190(1)$ Å, $\beta = 90.42(3)°$, and $Z = 2$] and is similar to that published for $(PEA)_2SnI_4$.[11] The organic cations continue to adopt the gauche conformation (Figure 4a) as in the fluoro analogue and are packed to form layers between the SnI_4^{2-} perovskite sheets. Within the inorganic layers, the two angles of the Sn−I−Sn units (the linkage between neighboring octahedra) are 155.0 and 154.5° and the average Sn−I bond length is 3.164 Å. Further information on the bond distances and angles for the inorganic layer in $(2\text{-ClPEA})_2SnI_4$ is summarized in Table 4.

The crystal of $(2\text{-BrPEA})_2SnI_4$ adopts a fully ordered monoclinic cell [$P2_1/c$, $a = 18.540(2)$ Å, $b = 8.3443(7)$ Å, $c = 8.7795(7)$ Å, $\beta = 93.039(1)°$, and $Z = 2$]. These parameters indicate an increased volume of the formula unit $(2\text{-BrPEA})_2SnI_4$ (678 Å^3) relative to that of $(2\text{-ClPEA})_2SnI_4$ (646 Å^3) and $(2\text{-FPEA})_2SnI_4$ (626 Å^3), which reflects the need to accommodate the different volumes of the halogen atoms. Note that the formula unit is contained in a box defined by the spacing between the inorganic layers (the height) and the squarelike unit (the base) shown in Figure 3. The interlayer spacing in $(2\text{-BrPEA})_2SnI_4$ [$18.54 \cdot \sin(93.04°) = 18.51$ Å] is substantially larger than those of the 2-F and 2-Cl cases (16.66 and 16.89 Å, respectively). On

(16) Dimitrakopoulos, C. D.; Purushothaman, S.; Kymissis, J.; Callegari, A.; Shaw, J. M. *Science* **1999**, *283*, 822.
(17) See: ref 1, p 44.

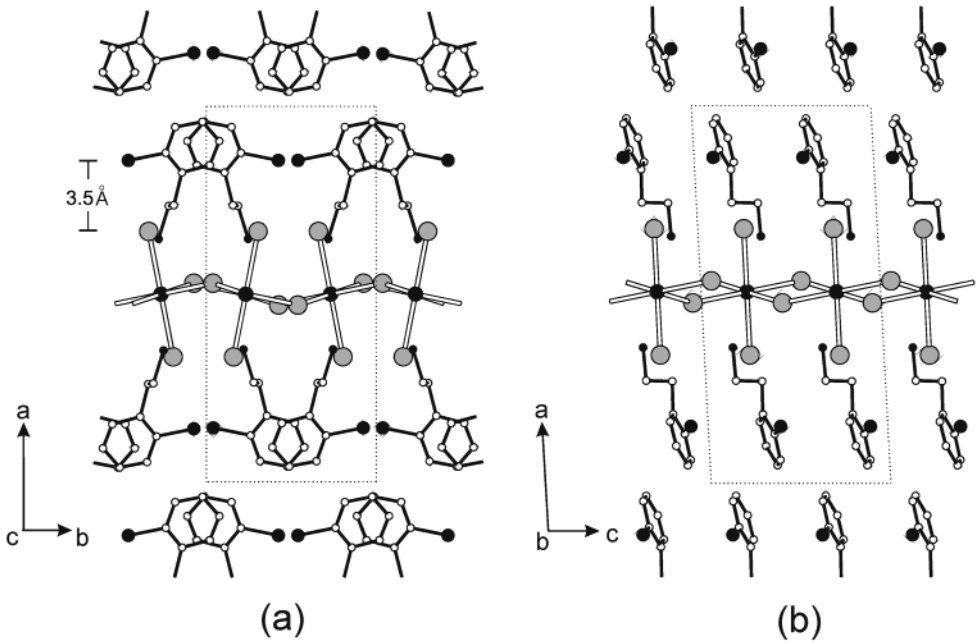

Figure 2. Crystal structure of (2-BrPEA)$_2$SnI$_4$ viewed along (a) the *c* axis and (b) *b* axis. Open bonds are used for the tin(II) iodide sheet, and filled bonds for the organic cations. Sn: large black sphere. I: gray sphere. C: small open sphere. N: small black sphere. Br: medium black sphere. The number (3.5 Å) refers to the distance between the plane of the bromine atoms and that of the apical iodine atoms.

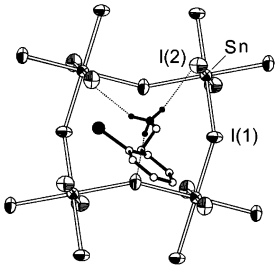

Figure 3. (2-Bromophenethyl)ammonium cation and the squarelike unit formed by four adjacent SnI$_6$ octahedra in (2-BrPEA)$_2$SnI$_4$. Atom labeling and thermal ellipsoids (50% probability) are given for the Sn and I atoms. Atoms of the organic cation are drawn as spheres of arbitrary sizes (C, unfilled; Br, large black; N, medium black; H from the $-NH_3^+$, small black). Dotted lines indicate the hydrogen bonds between the ammonium group and the iodine atoms.

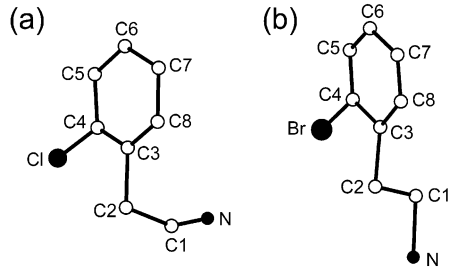

Figure 4. Organic cations with atom labels in the crystal structures of (a) (2-ClPEA)$_2$SnI$_4$ and (b) (2-BrPEA)$_2$SnI$_4$. Note the gauche conformation of the side chain in (a) and the anti conformation in (b).

the other hand, the area of the squarelike unit in (2-BrPEA)$_2$SnI$_4$ (36.63 Å^2) is relatively small compared with the 38.24 and 37.56 Å^2 values for (2-ClPEA)$_2$SnI$_4$ and (2-FPEA)$_2$SnI$_4$, respectively. The shrinkage of the squarelike unit in (2-BrPEA)$_2$SnI$_4$ is achieved mainly through further "bending" the Sn−I−Sn unit [bond angle 148.7°, as compared with 154.8° for 2-(ClPEA)$_2$SnI$_4$ and 153.3° for (2-FPEA)$_2$SnI$_4$]. Overall, the additional volume created for the Br atom is derived from an expansion of the interlayer spacing, which outweighs the slight contraction of the squarelike unit.

The expansion of the interlayer spacing in (2-BrPEA)$_2$SnI$_4$ appears to be closely related to the conformation of the organic cation—it adopts the anti conformation, whereas in both (2-ClPEA)$_2$SnI$_4$ and (2-FPEA)$_2$SnI$_4$ the gauche conformation is formed (Figure 4). Molecular modeling[18] shows that the anti conformer of the cation is significantly longer (6.7 Å) than the gauche form (4.9 Å). [Notice that the halogen substituent, when situated at the 2-position of the phenyl ring, does not affect the length of the organic cation, be it the gauche or anti conformation—the length of the molecule remains the distance between the N and C6 atoms (see the labeling in Figure 4).] The elongated anti conformation provides more potential for pushing apart the interlayer space and, therefore, seems to be a more advantageous choice for accommodating a bulky cation such as 2-BrPEA. Notably, calculations have shown that the gauche conformation of similar phenethylammonium-based cations is more stable than the anti conformation in the gas phase.[19] The crystal structure of (2-BrPEA)$_2$SnI$_4$, however, demonstrates that, in the solid state, the anti conformation can become the preferred structure in the context of molecular packing.[20]

Substituents at the 2-positions of the phenyl group are generally located close to the apical iodine atoms from the inorganic layer. For instance, in (2-BrPEA)$_2$SnI$_4$, the closest distance between the bromo group and the iodine atoms is 4.29 Å (van der Waals distance:[21] 3.9 Å); the corresponding

(18) Molecular simulation is carried out with the software of CS Chem3D Pro from the Cambridge Corp. The molecule is first drawn with the default bond lengths and angles. After "cleaning up" the structure, the conformation is optimized using the MM2 Force Field with default parameters.

(19) Urban, J. J.; Cronin, C. W.; Roberts, R. R.; Famini, G. R. *J. Am. Chem. Soc.* **1997**, *119*, 12292.

Cl···I distance in $(2\text{-ClPEA})_2SnI_4$ is 3.98 Å (van der Waals distance: 3.7 Å), and the F···I distance in $(2\text{-FPEA})_2SnI_4$ is 3.78 Å (van der Waals distance: 3.4 Å). To further illustrate the size effect of the halogen atoms on the crystal structure, it is useful to study the spacing between the plane of the halogen atoms and that of the apical iodine atoms, as this spacing should be most sensitive to the different halogen atoms. In $(2\text{-BrPEA})_2SnI_4$ the spacing is 3.50 Å (Figure 2); in $(2\text{-ClPEA})_2SnI_4$ it is 3.03 Å (Figure 1), and in $(2\text{-FPEA})_2SnI_4$, 2.43 Å. Again such monotonic change is in keeping with the sizes of the halogen atoms. The spacing can usually be adjusted through the orientation of the organic cations, as is the case in $(2\text{-ClPEA})_2SnI_4$ and $(2\text{-FPEA})_2SnI_4$ (e.g., the angle between the aromatic plane and inorganic sheet is 42.0 and 35.8°, respectively), whereas in $(2\text{-BrPEA})_2SnI_4$ the anti conformation of the organic cation presumably also helps widen the spacing between the bromine atoms and the apical iodine atoms.

Notable structural changes in the perovskite sheet of $(2\text{-BrPEA})_2SnI_4$ are also observed. First, the neighboring SnI_6 octahedra (linked by a basal iodine atom) are tilted relative to each other, so that the basal iodine atoms are shifted by 0.54 Å above or below the plane defined by the tin atoms (parallel to the 100 plane), causing the wavy pattern in the overall inorganic sheet as seen in Figure 2a. Note the apical Sn−I bonds are also tilted significantly (by 11.3°) from the normal of the plane of the tin atoms (Figure 2a). For comparison, in both $(2\text{-ClPEA})_2SnI_4$ and $(2\text{-FPEA})_2SnI_4$, the basal iodine atoms and the tin atoms are located practically on the same plane and the apical Sn−I bonds are closer to being perpendicular to the inorganic sheet (Figure 1). Second, as mentioned earlier, the Sn−I−Sn angle (148.7°) is more compressed as compared with those of $(2\text{-ClPEA})_2SnI_4$ and $(2\text{-FPEA})_2SnI_4$ (average values: 154.8 and 153.3°, respectively). Finally, the average Sn−I bond distance (3.148 Å) of $(2\text{-BrPEA})_2SnI_4$ is slightly shorter than those found in $(2\text{-ClPEA})_2SnI_4$ (3.164 Å) and $(2\text{-FPEA})_2SnI_4$ (3.159 Å). Other bonding details for the inorganic layer of $(2\text{-BrPEA})_2SnI_4$ are included in Table 5.

Finally, the packing and intermolecular interactions of the organic cations are depicted in Figure 5 for $(2\text{-BrPEA})_2SnI_4$. Within an organic cation layer, the aromatic units stack along the *c* axis to form columns, where the neighboring molecules are oriented in almost opposite directions. With the bulky bromine atoms thus tucked away, the neighboring aromatic rings approach one another, the resultant shortest C−C distance being 3.80 Å (van der Waals distance: 3.40 Å). Across the columns the bromine is located to a carbon atom at a distance (4.05 Å), somewhat close to the van der Waals distance (3.55 Å), whereas interaction between the bromine atoms (shortest distance, 4.49 Å; van der Waals distance, 3.70 Å) seems to be less significant. Stronger intermolecular forces exist between the layers. Here the shortest contact between the carbon atoms is found to be of 3.38 Å, indicating the typical aromatic−aromatic interaction. This interaction helps organize the aromatic groups from the two layers into parallel pairs, as shown in Figure 5b.

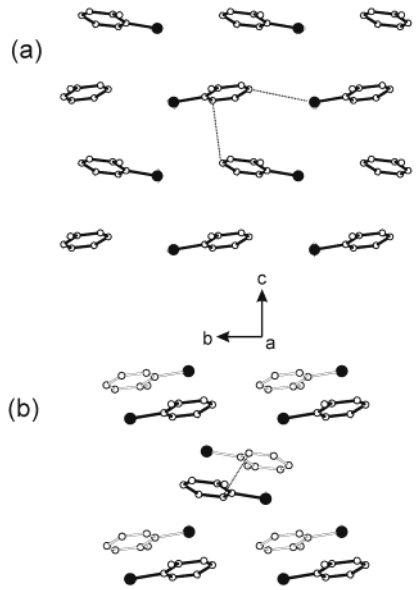

Figure 5. Packing of the 2-bromobenzyl groups in $(2\text{-BrPEA})_2SnI_4$ viewed along the *a* axis: (a) a single layer of the 2-bromobenzyl groups; (b) a double layer of 2-bromobenzyl groups from adjacent layers. Dotted lines denote the shortest intermolecular atom-to-atom distances. Molecules with black bonds are from the same layer as (a), and molecules with open bonds belong to the second layer. The terminal nitrogen atom and the adjacent carbon atom have been omitted for clarity.

Optical Properties. Optical absorption measurement proves to be effective in probing the electronic structures of the current semiconductive compounds. In particular, these hybrid materials exhibit sharp resonances in room-temperature optical absorption spectra, due to an exciton state associated with the band gap of the inorganic sheets.[6,7,22] Chemical modification of the organic cations often induces changes in the interactions between the organic and inorganic layers and, consequently, impacts the bonding and electronic structures of the inorganic sheets. Changes in the electronic structure are generally reflected in the shifts of the characteristic peaks in the optical spectra. As mentioned above, the bromination in $(2\text{-BrPEA})_2SnI_4$ produced rather significant deviation in the structures of the tin(II) iodide framework as well as the organic cation layer. It is interesting to see how the optical absorption features are affected as a result.

The room-temperature UV−vis absorption spectra of the thin films of $(2\text{-BrPEA})_2SnI_4$ and $(2\text{-ClPEA})_2SnI_4$ are shown

(20) The anti conformation is also found in crystals of $(PEA)_2CuX_4$ (PEA: phenethylammonium, X = Cl or Br), whereas, in $(PEA)_2SnI_4$, the same cation remains in the gauche form. The elongated anti form in the copper(II)-based systems seems to arise from a reason similar to that described in the text. In both $(PEA)_2CuX_4$ systems, the squarelike unit (areas: 26.73 and 29.68 Å^2 for the Cl and Br cases, respectively) of the inorganic sheet is significantly smaller than that of $(PEA)_2SnI_4$ (37.71 Å^2). To maintain sufficient volume for the PEA cation, larger interlayer spacings are therefore needed in $(PEA)_2CuX_4$ (19.31 Å for the Cl and 19.02 Å for the Br compound) relative to that of $(PEA)_2SnI_4$ (16.29). As in $(2\text{-BrPEA})_2SnI_4$, the longer anti conformers of the cation within $(PEA)_2CuX_4$ thus serve to further separate the inorganic sheets so as to contain the volume of the organic cations more effectively. For hybrid perovskites based on the Cu(II) halides, see: Willett, R. D. *Acta Crystallogr.* **1990**, *C46*, 565. For the crystal structure of $(PEA)_2SnI_4$, see ref 11.

(21) Bondi, A. *J. Phys. Chem.* **1964**, *68*, 441.

(22) Ishihara, T. In *Optical Properties of Low-Dimensional Materials*; Ogawa, T., Kanemitsu, Y., Eds.; World Scientific: Singapore, 1995; pp 288−339.

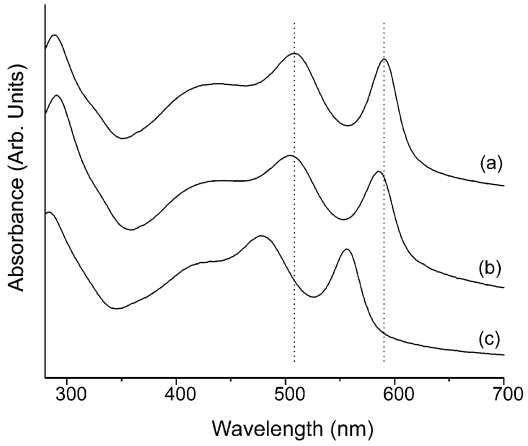

Figure 6. Room-temperature UV−vis absorption spectra for spin-coated thin films (on quartz disks) of (a) (2-FPEA)$_2$SnI$_4$, (b) (2-ClPEA)$_2$SnI$_4$, and (c) (2-BrPEA)$_2$SnI$_4$. The dotted lines highlight the shifts in the peak positions.

Table 6. Exciton Peak Wavelength, the Sn−I−Sn Bond Angles (Average), and the Sn−I Bond Lengths (Average) in Hybrid Perovskites Based on Cations of Aromatic Ethylamines

Cation	exciton wavelength, nm	Sn−I−Sn bond angle, deg	Sn−I bond length, Å
PEA[a]	609	156.5	3.144
4-FPEA[b]	609	156.4	3.151
NEA[c]	602	156.6	3.170
3-FPEA[b]	599	154.2	3.160
N5FPEA[d]	588	154.6	3.168
2-FPEA[b]	588	153.3	3.159
2-ClPEA[b]	586	154.8	3.164
2-BrPEA[b]	557	148.7	3.148
1-PYREA[e]	545	144.1	3.139

[a] Phenethylamine. See refs 11 and 13. [b] Substituted phenethylamine, abbreviated as *m*-XPEA: m = 4, 3, or 2; X = F, Cl, or Br. [c] (2-Naphthaleneethyl)amine; crystal structure to be published elsewhere. [d] 1:1 mixture of (2-naphthaleneethyl)amine and (pentafluorophenethyl)amine; crystal structures to be published elsewhere. [e] (1-Pyreneethyl)amine; crystal structure to be published elsewhere.

in Figure 6. Also included for comparison is the spectrum of previously reported (2-FPEA)$_2$SnI$_4$.[13] As can be seen, compound (2-BrPEA)$_2$SnI$_4$ shows a marked shift to higher energy in its exciton energy (557 nm, 2.23 eV), whereas the exciton energy of (2-ClPEA)$_2$SnI$_4$ (586 nm, 2.12 eV) remains close to that of (2-FPEA)$_2$SnI$_4$ (588 nm; 2.11 eV). Also noted is the corresponding shift for the band edge of the three systems. The difference in exciton energies is also reflected in the colors of the single crystals and powders: (2-ClPEA)$_2$SnI$_4$ and (2-FPEA)$_2$SnI$_4$ both are darker red, as compared with the lighter red coloration of (2-BrPEA)$_2$SnI$_4$.

The shift in the exciton energy suggests certain correlation with the Sn−I−Sn bond angle in the inorganic framework. Table 6 includes the exciton peak wavelengths and the corresponding Sn−I−Sn bond angles in a group of hybrid perovskites we have studied.[13] An overall trend can be readily distinguished, where larger Sn−I−Sn angles are in general associated with longer wavelengths (lower energies) of the exciton peaks and vice versa. Note in particular the unusually small Sn−I−Sn angles in (2-BrPEA)$_2$SnI$_4$ and (1-PYREA)$_2$SnI$_4$ and the correspondingly high energies of the excition states. The electronic properties of these materials are, however, subject to the influence from other structural factors

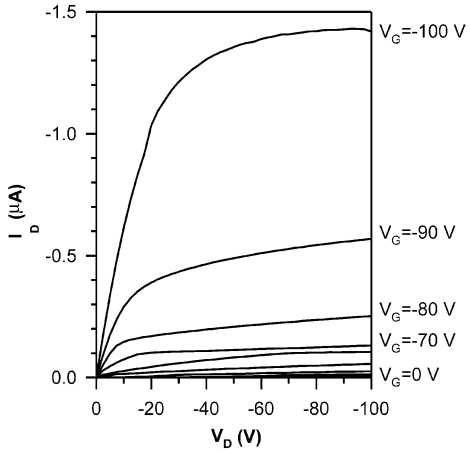

Figure 7. Drain current, I_D, versus source-drain voltage, V_D, as a function of the gate voltage, V_G, for a TFT with a spin-coated (2-BrPEA)$_2$SnI$_4$ channel of length $L = 9.5$ μm and width $W = 1500$ μm. The gate dielectric is 5000 Å SiO_2.

such as the hydrogen/ionic bonding between the ammonium group and the iodine atoms,[13] the dielectric modulation of the organic/inorganic layers,[23] and the grain size of the film,[24] which perhaps account for the observed small deviations from this trend. For comparison, we have also included in Table 6 the average Sn−I bond distance of the individual compounds. As can be seen, correlation between the exciton peak wavelengths and the bond distances appears less regular than that attained for Sn−I−Sn bond angles. Further theoretical study on band structures of tin(II) iodide networks would be helpful for elucidating the apparent correlation between the Sn−I−Sn angle and the exciton energy or band gap of these systems.

Previously, the shifts of excitonic bands observed in similar hybrid films based on MI_4^{2-} (M = Sn, Pb) sheets have been attributed to order/disorder effects in the crystallographic structure.[25] Therein, the authors claimed that ordered structures produce exciton energies distinct from those of the disordered structures and that, therefore, the exciton wavelength is indicative of whether the inorganic sheet is ordered or disordered. The data in Table 6, however, do not support such a claim. For example, the structures based on 4-FPEA, 2-BrPEA, and 1-PYREA are all solved in an ordered model of the same space group $P2_1/c$, and yet their exciton wavelengths range from 609 nm (4-FPEA) to 557 nm (2-BrPEA) and 545 nm (1-PYREA), which literally constitute the high end and low end of the exciton energies observed. Likewise, analogous hybrids solved with disordered crystallographic models yield a similar range of exciton peak wavelengths (e.g., 609 nm for the PEA cation and 586 nm for the 2-ClPEA cation). Furthermore, the data presented in ref 25 can also be rationalized by the currently proposed correlation between M−I−M bond angle and exciton wavelength. For example, the Pb−I−Pb angle is 148.5° in

(23) Hong, X.; Ishihara, T.; Nurmikko, A. V. *Phys. Rev. B: Condens. Matter* **1992**, *45*, 6961.
(24) Chondroudis, K.; Mitzi, D. B.; Brock, P. *Chem. Mater.* **2000**, *12*, 169.
(25) (a) Mousdis, G. A.; Papavassiliou, G. C.; Raptopoulou, C. P.; Terzis, A. *J. Mater. Chem.* **2000**, *10*, 515. (b) Papavassiliou, G. C.; Mousdis, G. A.; Koutselas, I. B. *Adv. Mater. Opt. Electron.* **1999**, *9*, 265.

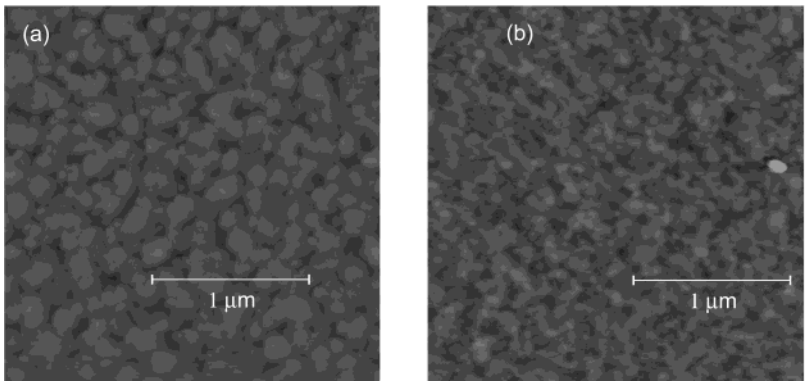

Figure 8. Atomic force microscope (AFM) topology images for spin-cast films of (a) $(2\text{-BrPEA})_2SnI_4$ and (b) $(2\text{-ClPEA})_2SnI_4$ on silicon substrates with 5000 Å of thermally grown oxide. Each film was imaged within the channel region of a similar TFT device.

the compound $[H_3N(CH_2)_6NH_3]PbI_4$ reported therein and its exciton wavelength is 482 nm, while the Pb−I−Pb angles in $[C_6H_5CH_2CH_2NH_3]_2PbI_4$ and $[C_{10}H_{21}NH_3]_2PbI_4$ (phase II) are larger (152.7 and 155.8°, respectively) and their exciton wavelengths are correspondingly longer (both ca. 510 nm).[25,26]

Thin-Film Field-Effect Transistors. Hybrid semiconductive perovskites provide a platform for combining the low-cost processing of organic materials and the high charge carrier mobilities of ionic/covalently bonded inorganic semiconductors.[2] The performance of TFTs based on the hybrid material as the channel layer generally depends on a number of factors such as the band gap of the semiconductive components, the interaction between the channel material and the electrodes, and the morphology of the thin film formed in the deposition process. Chemical modifications of hybrid semiconductors can influence one or more of these factors and thereby introduce a new dimension to the exploratory research on device fabrication. Presented here are the device characteristics of TFTs based on $(2\text{-BrPEA})_2SnI_4$ and $(2\text{-ClPEA})_2SnI_4$, as well as the film morphologies obtained from AFM (atomic force microscopy) studies.

The overall device characteristics of the TFTs based on $(2\text{-BrPEA})_2SnI_4$ are included in Figure 7, where a representative plot of drain current, I_D, versus source-drain voltage (source is always grounded), V_D, is shown as a function of the applied gate voltage, V_G. The p-channel TFT operates in accumulation mode upon application of a negative bias to the gate electrode, as the concentration of holes contributing to I_D increases. Application of a positive gate bias depletes the channel of holes, turning the device off. At low V_D, I_D increases approximately linearly with V_D, while, at high V_D, I_D saturates as the hole accumulation region in the channel is pinched off near the drain electrode.

The operation of the hybrid TFT is adequately modeled by standard field-effect transistor equations, as is also the case for organic TFTs.[27,28] Plots of I_D versus V_G at a constant low V_D based on Figure 7 yield a linear regime field-effect mobility, μ, of 0.030 $cm^2\ V^{-1}\ s^{-1}$ and an on−off ratio, I_{on}/I_{off}, of approximately 10^4. In the saturation regime, the same $(2\text{-BrPEA})_2SnI_4$-based TFT yields a maximum field-effect mobility, μ, of 0.086 $cm^2\ V^{-1}\ s^{-1}$, with a threshold voltage $V_T = -70$ V and an on−off ratio, I_{on}/I_{off}, of approximately 10^5. The difference between the linear regime and the saturation regime mobilities resembles that of the previous spin coated $(PEA)_2SnI_4$-based devices,[2] although it is smaller here. In general, difference between the linear regime and the saturation regime mobilities may be attributed to charge transport involving trap states. The mobilities of the current devices, both in the linear and saturation regime, are markedly lower than the corresponding values of $(PEA)_2SnI_4$-based devices. The reduced effective mobilities are likely to be at least partially attributable to the larger band gap of $(2\text{-BrPEA})_2SnI_4$, which makes it more difficult to inject charge carriers from the source/drain electrodes.

The TFTs based on $(2\text{-ClPEA})_2SnI_4$ showed lower performance than the $(2\text{-BrPEA})_2SnI_4$ devices. In the linear regime, the mobility is 2 orders of magnitude lower and the device shows a higher threshold voltage and lower maximum drain current. Similar comparison of device characteristics between $(2\text{-ClPEA})_2SnI_4$ and $(2\text{-BrPEA})_2SnI_4$ exists in the saturation regime.

As mentioned above, film morphology is an important factor that can affect device performance. AFM studies on thin films of the two compounds show substantially larger grain sizes for $(2\text{-BrPEA})_2SnI_4$ than for $(2\text{-ClPEA})_2SnI_4$. As is seen in Figure 8, almost all the grain sizes for the $(2\text{-ClPEA})_2SnI_4$ film are under 100 nm, whereas, for that of $(2\text{-BrPEA})_2SnI_4$, most grains are substantially larger than 100 nm. The larger grain sizes of $(2\text{-BrPEA})_2SnI_4$ may therefore be the reason for its better device performance mentioned above. Similar effects of grain size on TFT performance had been observed in the (fluorophenethyl)ammonium-based perovskites [$(m\text{-FPEA})_2SnI_4$, $m = 2$, 3, or 4],[13] where larger grain sizes were also associated with better device characteristics.

Conclusions

This paper describes our effort to use the steric effect from the organic cations to modify the crystal structures and

(26) (a) Calabrese, J.; Jones, N. L.; Harlow, R. L.; Herron, N.; Thorn, D. L.; Wang, Y. *J. Am. Chem. Soc.* **1991**, *113*, 2328. (b) Takahashi, J. Master Thesis, Tohoku University, 1989.
(27) Dimitrakopoulos, C. D.; Furman, B. K.; Graham, T.; Hegde, S.; Purushothaman, S. *Synth. Met.* **1998**, *92*, 47.
(28) Sze, S. M. *Physics of Semiconductor Devices*; Wiley: New York, 1981; p 442.

electronic properties of organic−inorganic perovskites. Our results show that larger variations in the bonding features of the inorganic sheet are effectively achieved when additional steric hindrance is introduced in its proximity [i.e., at the 2- position of the aromatic group in the prototypical $(PEA)_2SnI_4$]. The structural diversity provided by such studies makes it possible to correlate the crystal structures and electronic properties of these materials. Our current data generally support the notion[13] that a reduced Sn−I−Sn angle (further from 180°) correlates with a larger band gap, although the electronic structure is certainly influenced by various other factors as well. The steric effect also introduces new features in the organic component. Most remarkably, while the organic cation continues to adopt the more common gauche conformation in $(2\text{-ClPEA})_2SnI_4$ and $(2\text{-FPEA})_2SnI_4$, it switches to the elongated anti form in $(2\text{-BrPEA})_2SnI_4$. Apparently, the longer conformer is needed to create larger spacing between the inorganic sheets, so as to contain the additional volume from the Br atom.

Along the same line, one could imagine placing other bulky groups, either at the same 2-position on the phenyl group or on the side chain, so as to maintain the proximity to the inorganic layer. On the basis of the results from this study, one could expect the organic cation to retain an elongated conformation (e.g., the anti conformation) so as to produce enough space for the bulky groups. Also the inorganic sheet would likely show distortions similar to those observed in $(2\text{-BrPEA})_2SnI_4$. It is interesting to experimentally probe the limit of the steric tolerance of the layered structure, namely, to probe how large a substituent can be introduced without causing the perovskite sheet to break down. Such study is ongoing in our laboratory, to further study structure−property relations and to screen potentially useful semiconductive materials.

Acknowledgment. The authors thank Joanna Rosner and T. Graham for help with substrate preparation for the TFT devices.

Supporting Information Available: Full crystallographic data in CIF format for $(2\text{-ClPEA})_2SnI_4$ and $(2\text{-BrPEA})_2SnI_4$. This material is available free of charge via the Internet at http://pubs.acs.org.

IC0261474